Change detection in floodable areas of the Danube delta using radar images

Simona Niculescu, Cédric Lardeux, Jenica Hanganu, Grégoire Mercier, Laurence David

Change Detection in Floodable Areas of the Danube Delta Using Radar Images

Simona Niculescu[a], Cédric Lardeux[b], Jenica Hanganu[c], Grégoire Mercier[d], Laurence David[a]

a. Laboratoire LETG-Brest, Géomer - UMR 6554 CNRS - Rue Dumont d'Urville, Technopôle Brest - Iroise, F-29470 Plouzané, France
simona.niculescu@univ-brest.fr, tel 0033298498616, fax 0033298498703
b. Office National des Forêts - 2, avenue de Saint-Mandé, 75570 Paris Cedex 12
c. Danube delta for Research and Development, 165 Babadag street, Tulcea 820112, Romania
d. Institut Télécom, Télécom Bretagne, Lab-STICC/CID - UMR 6285 CNRS - Technopôle Brest - Iroise; CS 83818, F-29238 Brest cedex – France

RESUME

Dans le delta du Danube, le risque d'inondation est un risque majeur. Depuis les années 2000, la zone humide côtière du delta a été frappée par des inondations en 2002, 2005, 2006 et 2010. En partant d'une série de données hydrologiques et d'observations satellite de 2009 et de l'été 2010, on utilise dans cet article l'information et les observations sur l'occupation du sol, notamment dans le domaine de l'inondable, pour étudier la problématique de la prévision du risque. L'un des objectifs principaux de la méthodologie développée consiste en la mise en œuvre de différents types de données pertinentes pour ce type d'analyse en proposant une chaîne méthodologique spécifique pour la détection du changement en termes de risque d'inondation. Les données du satellite japonais ALOS sont utilisées pour présenter une démarche méthodologique de traitement de données radar multidates fondée sur une analyse de l'entropie temporelle permettant de détecter des changements dans les zones inondables du delta du Danube.

ABSTRACT

In the wetlands of the Danube delta floodplain, flooding is a major natural risk. The coastal wetlands have been seriously impacted by floods in 2002, 2005, 2006 and 2010. Using hydrological and satellite observations acquired in 2009 and during the summer of 2010, this paper tackles the issue of forecasting risk based on land cover information and observations. A major objective of this methodological work consists in exploring several types of data from the Japanese ALOS satellite. These data are used to illustrate a multitemporal radar data processing methodology based on temporal entropy analysis that enables change detection in the floodable areas of the Danube delta.

MOTS-CLES: delta du Danube, risque d'inondation, détection du changement, entropie temporelle, satellite ALOS, prévision, zone inondable.

KEYWORDS:

Danube delta, flood risk, change detection, temporal entropy, ALOS satellite, forecasting, floodable areas

1. Introduction

Assumptions related to global warming and its effects engender significant preoccupations with regards to the rise in heavy rainfall occurrences, despite numerous doubts that still exist concerning the rainfall response to global warming. In this respect, climate change may increase flooding and other risks throughout the whole water cycle in the years to come. Extreme weather conditions, such as heavy rains causing flash floods, are expected to become more frequent throughout Europe. Climate change is also expected to lead to a rise in the sea level (from 26 to 82 cm in 2100, IPCC, 2014) and shoreline erosion and, when accompanied by strong storm waves, will threaten low altitude coastal towns, which will be more likely to be flooded. According to GIEC, this phenomenon will most likely affect up to 1.6 million more Europeans by 2070. The rise in sea level will also be damaging for the coastal wetlands.

The geographical landscape dealt with in this paper refers to deltas, i.e., recently formed ever-changing environments that are part of the shoreline and wetlands and that are influenced by absent or weak tides. These are generally characterised by salinity variations –freshwater from the river on the one hand and marine saltwater on the other hand – as well as by considerable biomass and productivity, due mainly to the abundance of nutrients present in the water and sediments. Despite their indisputable importance, these environments remain among the most endangered ecosystems in the world because of land reclamation, drying out, pollution or overexploitation of resources. The Danube delta, a coastal wetland of the Black Sea, cannot escape these dangers, and, to preserve its resources, it has been declared a Biosphere Reserve (MAB-UNESCO) (in 1993). The Danube delta is a representative flood hazard site as it has been affected by climate-related floods and hence by systematic rises of the water level.

Radar satellites are extremely useful for characterising and mapping flood risks because of their ability to collect data and images through the cloud cover that usually accompanies floods. SAR sensors are able to detect flooding because flat surfaces reflect the signal away from the sensor, decreasing the amount of returned radiation (Gan et *al.*, 2012). The crisis management phase involves the production of map documents, which localize the event and its extent. There are several methods for obtaining an information plan concerning space data, such as photo-interpretation and image segmentation, which make use of mathematic principles, such as contour detection, fuzzy logic with data mining or artificial neural networks. Many SAR image-processing techniques exist that have more or less successfully derived flood area or extent, including simple visual

interpretation (Oberstadler and *al*., 1997), image histogram thresholding (Brivio et *al*., 2002; Matgen et *al*., 2007, 2011), automatic classification algorithms (Bonn and Dixon, 2005; Inglada and Mercier, 2007; Martinis et *al.*, 2009; Niculescu et *al*., 2009), image texture algorithms (Schumann and *al*., 2009), and mulitemporal change detection methods (Laugier et *al*., 1997; Niculescu et *al*., 2009, 2010) ; the application of neural networks in a grid system (Kussul et *al*., 2008), fractal dimensioning of multi-temporal images (Huang et *al*., 2011), pixel-based segmentation (Martinis et *al*., 2009), and statistical active contouring (Horritt et *al*., 2001). In the Danube delta research has been carried out by exploiting radar imagery ENVISAT/ASAR and hyperspectral imagery CHRIS/PROBA for mapping flooded and floodable areas during the events of spring 2006 (Niculescu et *al*., 2010). This research focused on the methodological aspects related to the characterization of the *flood hazard* and modeling of the *Land cover*. The method of kernels, particularly adapted to the highlighting of the special-temporal variations - Support Vector Machine – and the methods based on the principle of the vague logic (object-oriented classifications) have been developed.

The purpose of this paper is to use the Japanese ALOS satellite, specifically the PALSAR microwave radar (*Phased Array type L-band Synthetic Aperture Radar*) with 15-m resolution, thereby permitting the discrimination of floodable areas. Change detection by temporal entropy based on radar images is the methodology proposed in this paper.

2. Study Area

The Danube crosses Europe from Germany to the Black Sea, where it forms the second largest delta in Europe following the delta at the mouth of the Volga. The Danube delta area covers 4 455 km^2, and 79 % (i.e., 3 510 km^2 without the Razim-Sinoe lagoon complex) of the delta area is located in southeastern Romania (figure 1). The Romanian portion of the delta is divided between the inland water area and the maritime area (figure 1). The inland section is located westward from a line connecting the Letea dunes (Periprava Village) with the Dunavat peninsula. The maritime section begins at the alignment of the Letea Caraorman and Crsanicol marine levees and runs all the way to the Black Sea.

Reeds are an essential component of the deltaïc landscape, and *Phragmites australis* is the dominant species in the entire Danube delta. It is also accompanied by other hydrophilic species[1]. The combination of these plants varies, and there are different plant communities. Hanganu *et al.* (2002) defined four main communities[2] that differ depending mainly on the soil types, pH, flooding conditions and salinity. The ecological dynamics of the reed beds can be characterised by several types of plant cover, each enjoying its own dynamics in the ecological sequence process. This process is mainly driven by the water levels, as it may be accelerated or stopped by events such as floods (2006, 2010) or drying out periods (2007, 2011).

Our study site is located around Caraorman: the Caraorman fishing village, where fishermen berth their boats, the village and forest bearing the same name (figure 1). The village was set up on the Caraorman levee, 12 m above sea level.

Figure 1.
The Danube delta and geographical location of the training sample. Limit of internal/maritime part of the delta

[1] *Typha angustifolia, Schoenoplectus lacustris, Sparganium sp. and Thelypteris palustris.*
[2] *Phragmitetum communis, Scipo-Phragmitetum, Bolboschoeno-Phragmitetum and Astero tripolii-Phragmitetum.*

At the outset, the hydrographic network of the delta is formed by three main arms: the Chilia arm (120 km long), which forms the natural border between Romania (south) and the Ukraine (north), the Sulina arm (64 km long) in the middle and the Sfantu-Gheorghe arm to the south, currently 70 km long. The first interventions in the water system of the Danube distributaries date back to 1857-1858, after the creation, in 1856, of the European Commission of the Danube (ECD). Sulina (in the middle of the delta) was the distributary channel altered between 1857 and 1902. Due to the cut-off operations performed on the meanders of this distributary channel, more precisely on the « big M » (DunareaVeche), the distributary channel was shortened by 20.8km. Thus, its length decreased from 83.4km to 62.6km, whereas its depth increased from 2.4m to 7.2m. The Sulina distributary channel development also required the reinforcement of the Danube River banks, and the building of a jetty at the river mouth in the Black Sea. This jetty prevents aggradation by sediments carried by the Chilia distributary channel.

The delta plain is characterised by minor altitude differences: 20.5 % of the delta is below the 0 level of the Black Sea, 54.6 % is between 0 and 1 m, 18.2 % is between 1 and 2 m and only 6.7 % is above 2 m of altitude. The low-lying areas between the Chilia-Sulina and Sulina-Sfantu-Gheorghe arms harbour many delta lakes that cover 8.9 % of the whole delta area (Gastescu and Stiuca, 2008). These lakes play an important role during rises in the Danube level, as the excess water accumulates in them and then flows into the main arms when the water level is low. Another characteristic of this deltaic environment is the existence of ecosystems consisting of reed beds, mainly *Phragmites australis*. These reed beds make up a considerable part of the floodable delta, and they are also thought to be the largest uninterrupted reed beds in the world.

Despite the moderate rainfalls in this area, the Danube delta is flooded every year. The historical analysis of the maximum discharge of the Danube (figure 2) in Tulcea reveals that considerable river discharges were recorded in 1895 (13 700 mc/s), 1942 (13 387 mc/s), 1970 (14 520 mc/s), 1974, 2003, 2006 (15 900 mc/s) and 2010 (16 600 mc/s). The annual multi-analysis (1931 – 2011) of the Danube water levels at the entrance of the delta (in Tulcea) (figure 2) also shows that most of the maximum river discharge episodes occur from March to July. The last two major flood rises, which occurred in 2006 and 2010 (figure 2), were preceded by heavy snowfalls during the winter and by relatively early snow melting on the mountains in the catchment area of the Danube. In July, the Danube level decreases significantly down to low levels and discharge rates at the end of summer and beginning of autumn (from August to February) (figure 2). According to these data, the floods of

2006 and 2010 were followed by periods of considerable low water (figure 2). In Tulcea, the Danube level was 1 m in August 2007 and 0.35 m in October 2011.

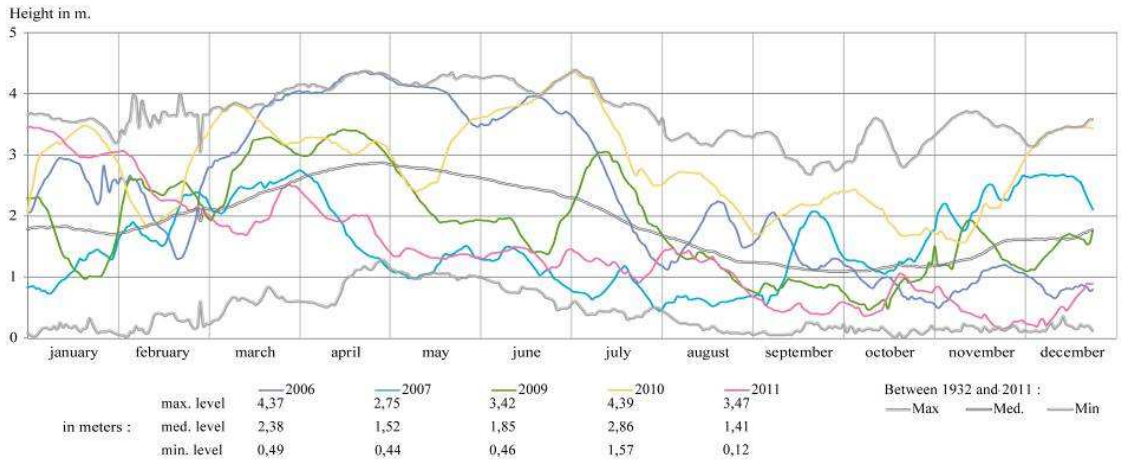

Figure 2.
Danube daily levels at Tulcea in 2006, 2007, 2009, 2010 and 2011. Mean daily levels from 1931-2011.

The floods of 2010 affected more than 30 counties and 400 localities in the northern and eastern portions of Romania, the Danube delta included. More than 16 500 people were evacuated and more than 45 000 hectares of agricultural land and forests were submerged.

3. Dataset

The satellite data included in this paper were acquired by the PALSAR instrument on the ALOS satellite. The ALOS (*Advanced Land Observing Satellite*) Japanese satellite was launched on 24 January 2006 and ceased to operate on 22 April 2011. It included two optical sensors and the PALSAR (*Phased Array type L-band synthetic aperture radar*) radar. The SAR concerned by this research operates at 1.27 GHz or 23.6 cm (L band; ALOS-PALSAR). The ALOS-PALSAR operating in the polarimetric mode uses a 14 MHZ bandwidth, providing a 11m optical range resolution or a 30-meter ground resolution with a 20° incidence angle.

The Phased Array type L-band Synthetic Aperture Radar (PALSAR) is an active microwave sensor using the L-band frequency (24 cm) to achieve cloud-free and day-and-night land observations. PALSAR is a fully polarimetric instrument, operating in fine-beam mode with single polarisation (HH or VV), dual polarisation (HH+HV or VV+VH), or full polarimetry (HH+HV+VH+VV). This paper focuses on dual polarisation data (dual HH and HV mode) (table 1).

Table 1.

ALOS/PALSAR satellite data used

RADAR sensor instrument	Before / during / after the floods	Acquisition day	Technical characteristics	Danube water level at Tulcea
Japanese ALOS satellite PALSAR sensor	Before	15 June 2009	Dual mode: HH, HV L-Band: 24 cm Resolution: 15 m x 15 m	2.52 m
		20 May 2010		3.70 m
	During	18 June 2010		4.37 m
	After	3 August 2010		3.06 m

The dual polarimetric mode allows image acquisition in two different linear polarisation modes. The alternation between the two polarisation configurations occurs on each individual impulse, which accounts for the phase difference between the two acquisitions.

The main objective of a RSO oriented towards applications such as the characterization of various flood prone areas or flooded areas, or the determination of different biophysical parameters of the land, is to detect by the measurements performed the quantities that best express the backscattering characteristics of the analyzed land. The backscattering coefficient is referred to when dealing with a SAR with any radar polarisation configuration.

Other types of data were used: the daily Danube levels in Tulcea in 2006, 2007, 2009 and 2010, the multi-annual mean of the Danube levels in Tulcea between 1931 and 2011, as well as the phenological reed calendar in the Danube delta (figure 5).

4. Methods

To detect the various types of surface changes resulting from the floods of 2010 in the Caraorman deltaic section and to characterise the floodable class by means of its backscattering mechanisms, we propose the following methodological analysis and image processing sequence: polarimetric indices extraction and implementation, calculation of the temporal entropy of the polarimetric indices, temporal entropy classification using support vector machine (SVM) and mono-temporal floodable class classification, using all the polarimetric indices (table 2) used.

Table 2.

Methodological sequence applied to ALOS/PALSAR images

Radar Dataset ALOS / PALSAR	**Danube water levels at Tulcea**	**Processing steps**	**Objectives**

<table>
<tr><td rowspan="2">06/15/2009</td><td rowspan="2">Normal condition (June 2009)</td><td rowspan="2">2.52 m</td><td rowspan="3">Orthorectification

Data filtering

Polarimetric indices

Temporal entropy of the polarimetric indices</td><td rowspan="3">HH, HV intensities and Polarimetric entropy</td><td>Analysis of polarimetric change between the 2 dates</td></tr>
<tr><td>Change indicators (entropy) applied to polarimetric indicators</td></tr>
<tr><td>06/18/2010</td><td>Floods (June 2010)</td><td>4.37 m</td><td>Change characterisation (stable classes, changing classes)</td></tr>
<tr><td colspan="3">Image resulting from temporal entropy</td><td>Entropy SVM classification</td><td>Classification into two classes: no change and radical change</td><td>Risk class detection (floodable areas): hydrophilic vegetation, halophilic vegetation, psammophilic vegetation

Stable class mask</td></tr>
<tr><td>06/15/2009</td><td>Normal condition (June)</td><td>2.52 m</td><td rowspan="4">Mono-temporal SVM classification</td><td rowspan="4">Diachrony analysis of the 4 dates</td><td>Floodable area detection based on the thematic mask extracted relying on the flooded areas of 18 June 2010 (Short vegetation (grassland), hydrophilic vegetation, psammophilic vegetation, mixed vegetation, mixed phragmites, forest, dominant phragmites, cut phragmites)</td></tr>
<tr><td>05/20/2010</td><td>Flood onset</td><td>3.70 m</td><td>Flooded area detection</td></tr>
<tr><td>06/18/2010</td><td>During</td><td>4.37 m</td><td>Flooded area detection and thematic mask of these areas</td></tr>
<tr><td>08/03/2010</td><td>After</td><td>3.06 m</td><td>Floodable area detection and characterisation</td></tr>
</table>

Two major types of polarimetric indices can be extracted from fully polarised data or from dual polarisation data. Coherent indices are well suited for target studies such as buildings for example whereas incoherent indices are better for distributed target such as grasslands, reeds or forest areas. Thus, because of the incoherent nature of the study classes, we will focus only on incoherent polarimetric indices.

Polarimetry relies on the vector-like nature of the wave (Papathanassiou and Cloude, 2001). It is designed to characterise targets by recording their responses in different radar wave emission and reception polarisations. To allow the separation of backscattering mechanisms in the same resolution cell and different incoherent target decomposition was developed as Cloude-Pottier (Entropie/Alpha), Van Zyl (Van Zyl, 1989, Cloude and Pottier, 1997), Freeman (Freeman and Durden, 1998) and Yamaguchi (Yajima et al, 2008).

As for double polarisation (fine beam dual mode), only the S_{hh} and S_{hv} terms are recorded coherently, thus reducing the polarimetric information acquired.

Starting from the K_{DP} target vector, the covariance matrix is expressed as follows:

$$\boldsymbol{k_L} = \begin{pmatrix} \boldsymbol{S_{hh}} \\ \boldsymbol{S_{hv}} \end{pmatrix} \quad \textbf{(1)}$$

$$\boldsymbol{C} = \boldsymbol{k_L}.\boldsymbol{k_L^*} = \begin{pmatrix} \boldsymbol{S_{hh}} \\ \boldsymbol{S_{hv}} \end{pmatrix}.(\boldsymbol{S_{hh}^*} \quad \boldsymbol{S_{hv}^*}) = \begin{bmatrix} \boldsymbol{S_{hh}S_{hh}^*} & \boldsymbol{S_{hv}S_{hh}^*} \\ \boldsymbol{S_{hh}S_{hv}^*} & \boldsymbol{S_{hv}S_{hv}^*} \end{bmatrix} \textbf{(2)}$$

$$\begin{aligned} \boldsymbol{S_{hh}} &= \boldsymbol{A_{hh}}.\boldsymbol{e^{j\varphi_{hh}}} \\ \boldsymbol{S_{hv}} &= \boldsymbol{A_{hv}}.\boldsymbol{e^{j\varphi_{hv}}} \end{aligned} \quad \textbf{(3)}$$

where

$$\boldsymbol{S_{hh}S_{hh}^*} = \boldsymbol{A_{hh}}.\boldsymbol{e^{j\varphi_{hh}}} \times \boldsymbol{A_{hh}}.\boldsymbol{e^{-j\varphi_{hh}}} = \boldsymbol{A_{hh}^2}.\boldsymbol{e^{j(\varphi_{hh}-\varphi_{hh})}} = \boldsymbol{A_{hh}^2} = \boldsymbol{I_{hh}} \quad \textbf{(4)}$$

S_{hh} and S_{hv} are the matrix terms corresponding to the HH and HV polarisations, respectively. A_{hh} and A_{hv} are the amplitudes of the two polarisations, whereas φ_{hh} and φ_{hv} are their phase, respectively.

This configuration allows extraction of the $H_{DP}/A_{DP}/\alpha_{DP}$ parameters (Cloude, 2007). In this paper we will investigate only H_{DP}.

Given that polarimetric ***entropy*** $\boldsymbol{H_{DP}}$ characterises the level of depolarisation of the backscattered wave, entropy can be calculated pixel by pixel using a linear combination of the image cross-variance matrix values.

$$\boldsymbol{H_{DP}} = -\sum_{i=1}^{2} \boldsymbol{P_i log(P_i)} \quad \textbf{(5)}$$

where $\boldsymbol{P_i} = \frac{\boldsymbol{\lambda i}}{\sum_{i=1}^{2} \boldsymbol{\lambda i}}$ and λ_i are the specific vectors of the coherency matrix.

In a second stage, the temporal analysis of some polarimetric indices (HH intensity, HV intensity and polarimetric entropy) using temporal entropy (Fuchs, 2008) is conducted using this equation:

$$H_{Temp} = -\sum_{\mathbf{i=1}}^{\mathbf{n}} \mathbf{P_i log(P_i)} \quad \textbf{(6)}$$

where $\boldsymbol{P_i} = \frac{\boldsymbol{Bi}}{\sum_{i=1}^{n} \boldsymbol{Bi}}$ and B_i correspond to the B indicator (HH, HV or polarimetric entropy in our case) observed on date n.

Therefore, temporal entropy has the same definition as polarimetric entropy, the only difference being that temporal entropy measures the heterogeneity undergone by the same index throughout time. This heterogeneity could be interpreted by change detection in the temporal point of view. As all Entropy, temporal entropy is range between [0,1].

Thus, a low temporal entropy (close to 0) means that the indicator used is stable in time. On the other hand, a high entropy value, close to 1, shows that the indicator has undergone a significant change through time.

Moreover, we suggest a comparison between the temporal entropy of HH, HV and polarimetric entropy to be able to characterise their changes. It is well known that HH polarisation allows the characterisation of the double rebound importance, where HV polarisation is particularly characteristic of the volume reflections. Thus, the temporal analysis of these polarisations together with the analysis of their polarimetric entropy will enable us to characterise the Danube water level evolution. Given that the Danube delta is mainly covered by reeds, the water level variation and the reed density variation are characterised by a significant double rebound modulation and volume backscattering mechanism.

Thus, the temporal analysis of HH and HV entropy reveals values that can characterise the state of the changes affecting the studied areas. In some areas, before the floods of 18 June 2010, the HH intensity was -7.7 dB, whereas the HV intensity was -15.5. During the floods, the HH intensity was -12.5 dB versus -26.7 dB for HV polarisation. This shows that intensity decreases during flooding, which means that the water response increases contrary to volume and double bounce scattering mechanisms. Therefore, in the delta, we can observe many different temporal signatures, which are shown in figure 3 in the Results and discussion chapter.

Based on these different indicators we apply change detection processing. Lu et al. (2004) classify the change detection methods into six categories: algebraic, transformation, classification, advanced, GIS approach, visual analysis and other techniques. Among these categories, several authors have published change detection method assessments, for instance Singh (1989), Lunetta and Elvidge (1998), Mas (2000), Jensen (2004) and Lu et al. (2004), Inglada and Mercier (2007), Quin et al. (2012).

In order to detect the changes and to characterize the type of area subjected to flooding we chose to use the supervised SVM (Support Vector Machines) classification algorithm. SVM allow us to produce a land cover change map as well as a land cover map. In case of land cover change map we used only temporal entropy whereas for the land cover map we used only polarimetric indicators for each date.

The algorithm used was SVM based on the kernel theory, which allows the settlement of problems that area linearly inseparable. It also allows the taking into consideration of numerous and heterogeneous parameters. The purpose of the SVM algorithm is to calculate the best separating hyperplane between two classes or, similarly, to maximise the margin between the study classes, more details are given in Burges (1998). Thus, SVM are

particularly relevant because SVM do not take into account any distribution assumptions. In addition, using the RBF[3] kernel of SVM allows classifying non-linear classification problems.

The presence of noise in the data can be taken into account by defining a distance allowing a certain data dispersion, thus relaxing the decision-making constraint (Lee et *al*., 1999; Lee et *al*., 2009).

The SVM principle was developed for a two-class problem, yet it may be extended to a higher number of classes according to the "one against one" (OAO) algorithm. This algorithm consists of the development of $\frac{Q(Q-1)}{2}$ hyperplanes separating each pair of classes. The final label is the one that was most commonly retained.

Where *Q* is the number of study classes.

In order to optimize RBF kernel, we used a cross validation process that gives us best results with $\sigma = 0.5$ and a cost parameter equal to 1000.

5. Results and Discussion

Microwave radiation polarisation, just like radar beam incidence angle and wave frequency, has been long acknowledged as an important parameter for object recognition and understanding object features. Access to the scattering matrix allows several analytical approaches and hence various ways of assessing the potential of multi-polarized radar images. One approach consists of synthesizing pixel-based signal strength, which should have been measured at the same frequency for any polarisation configuration (linear and/or circular). The images thus created may be considered analogically different channels from the channels of a multispectral image. We began by testing the ability of multi-polarized images to recognize various wetland classes and/or plant formations representing the flood-prone and flooded areas of our study area. A flooded area (on the image of 18 June 2010) is typically very dark because of the specular reflection caused by the smooth water area or, on the contrary, very bright in case of emerging vegetation (trees or grass), which causes double-bounce backscattering. The rich *Phragmites communis* canopy biomass reduces the floodable area delimitation precision, as it prevents the incident signal from reaching the flooded area. The occurrence of emerging vegetation complicates swamp and marsh shoreline detection. Detailed vegetation class recognition within these areas is a little more difficult if one relies solely on radar signal amplitude. Three groups of objects can be distinguished, which are more or less

[3] The Radial Basis Function (RBF) kernel

clearly detectable (on the image of 15 June 2009). The first group includes mainly shrubs or herbaceous species, which clearly distinguish themselves from the other plant formations. This may be considered to be an important contribution of the HV channel. Herbaceous swamps may be confused with psammophilus species. There is also some confusion concerning forests on dry substrates. The HH and HV channels do not allow distinguishing between several classes of flooded or non-flooded hydrophilic vegetation (reed mistaken for Thypha and Carex). It is also impossible to distinguish salty vegetation classes from other vegetation classes.

We suggest the extraction of the polarimetric parameters in order to better characterize especially the flood prone areas. These breakdowns provide access to a series of pixel-based or pixel group-based parameters (anisotropy, entropy (in our case), polarimetric phase, etc.) which are generally closely connected with the electric and geometrical features of the targeted elements. In principle, polarimetric breakdowns allow the detection of backscattering mechanisms the superposition of which gives rise to radar measured signals. The association between these mechanisms and the geometrical structure and dielectric features of the analyzed areas may thus enable their identification.

Using two-colour composites (figure 5a), combining HH and HV intensity with entropy, we propose the calculation of the entropy between two images, the first acquired on 15 June 2009 and the second on 18 June 2010 (figure 5a), to detect the changes that occurred between the two dates.

Indeed, the more important dynamic classes, such as the flooded and floodable classes, are approached through the diachronic analysis of the three dates considered important for these floods: 20 May 2010, 18 June and after the events of 3 August 2010. The date of 15 June 2009 (figure 3) is used to define the floodable classes due to its very low water level in relation to the thematic mask of the flooded areas extracted from the image of June 18 2010 (figure 4), when the floods reached their spatial extent peak. June 18 2010 saw the widest amount of flooded areas, especially in Caraorman Village, and the floods that were mainly due to groundwater oversaturation (rainfall floods) (figure 4).

Dominating reed

Tree Vegetation in floodable area

House to Caraorman

Mixed Vegetation

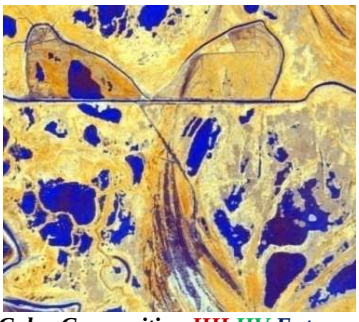

Color Composition HH HV Entropy. June 15, 2009

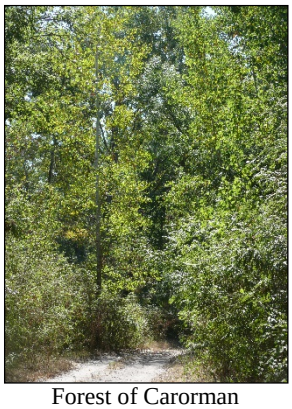

Forest of Carorman

Figure 3.
June 15, 2009. Colour composition and photos of the main classes of land cover of the flood areas

House flooded near the forest of Caraorman

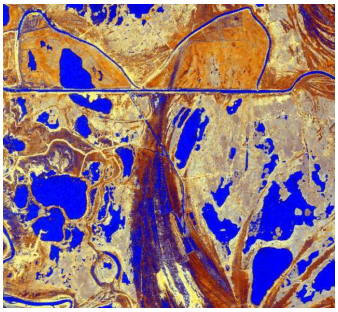

Colour composite HH HV entropy for June 18, 2010.

House located on an arm of Danube near Carorman

Flooding of the center of the locality Carorman

Flooding of the main street of the locality of Caraorman (a)

Flooding the main street of the locality of Caraorman (b)

Figure 4.
June 18, 2010. Colour composition and photos of flooded areas

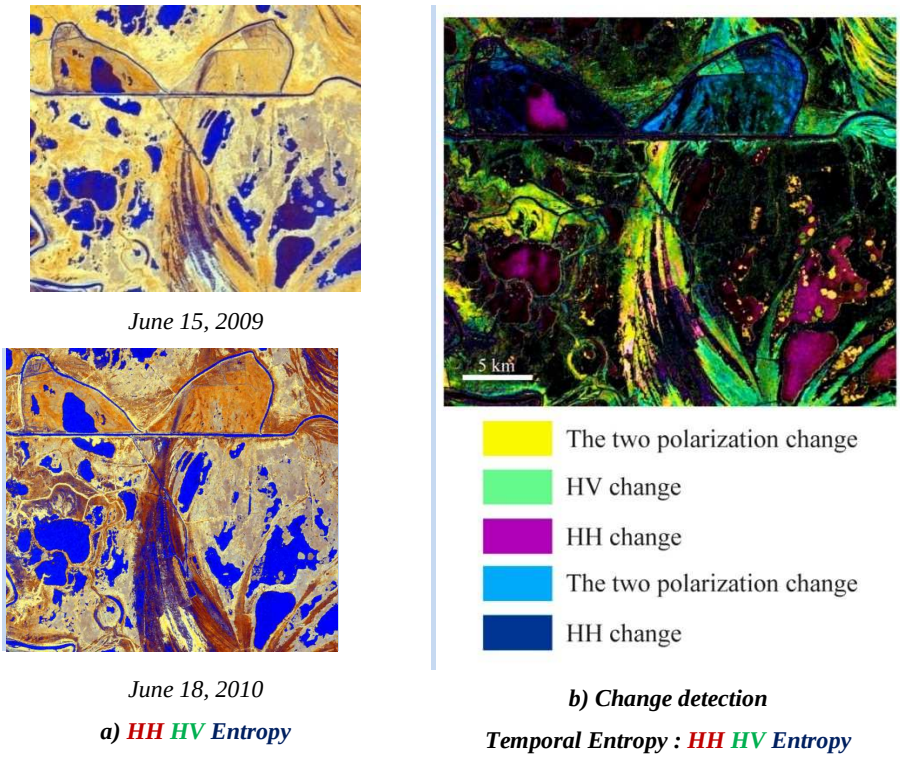

Figure 5.
Temporal entropy. Change detection between June 15, 2009 and June 18, 2010.

In the resulting image (figure 5b), the lighter the colours are, the more numerous the changes recorded. Therefore, yellow expresses a large number of changes, indicating that the two polarisations change. Green indicates a HV polarisation change, whereas magenta reveals a stable HV polarisation and a considerable HH change. Cyan indicates a change in the two polarisations, and blue expresses HH change compared with HV. Bearing in mind that the polarimetric information is closely related to the backscattering mechanism, the changes actually reflect the backscattering mechanism changes depending on the changes affecting the studied areas (figure 5b).

To better characterise the backscattering mechanism and hence to detect changes occurring in these areas depending on the Danube level changes and on the ground vegetation changes (*Phragmites spp.* in particular) before and during the floods, we propose an analysis of the major changes between the two polarisations in the various colour composites illustrated by diagram of figure 4. The different colours used in this diagram correspond to the colours shown in figure 3b (temporal entropy).

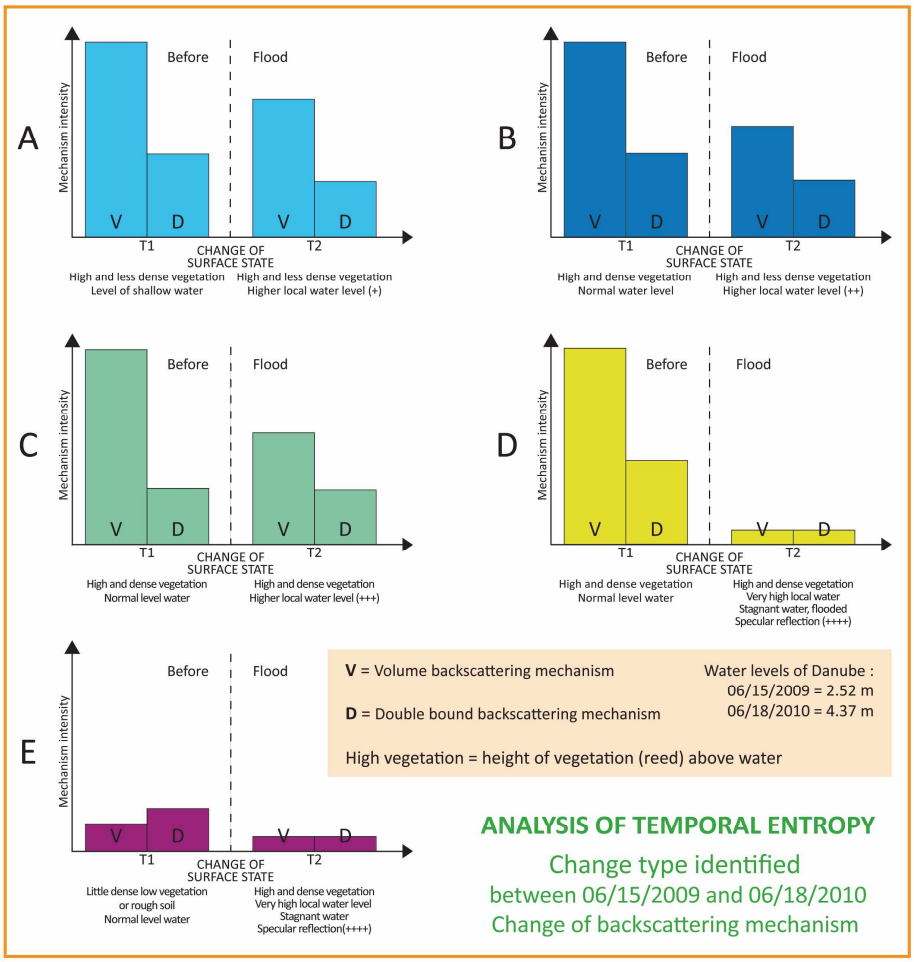

Figure 6.
Analysis of temporal entropy.

Relying on the field knowledge acquired in connection with the monitored areas and with the characteristics of volume backscattering and double bounce in double mechanisms, we distinguished between two types of areas in our analysis: the local water level and the vegetation. Area that appear in cyan blue in figure 5b means that the volume backscattering and double bounce mechanisms are more significant for the date prior to the floods (diagram A in figure 6). The areas associated with these backscattering mechanisms correspond to high and less dense vegetation with low water level (2.5 m) before flood and higher local water level (+) after flood. Diagram B corresponding to blue areas in figure 5b have similar behaviour as in diagram A except that the volume backscattering is lower during flood. This means that water levels are higher during the flood compared to diagram A. Areas in green in figure 5b means that HV backscattering level is strongly decreases between floods (diagram C in figure 6). This characterises high and dense vegetation areas where the water level increased

significantly (++) during the flood. Area that appears in yellow (figure 5b) correspond to areas covered by high and dense vegetation totally flooded during the event (+++). The important volume scattering and moderate double bounce scattering before the event decrease considerably during the flood. In the case of magenta area in figure 5b, this means that backscattering mechanisms are low in two cases but specular at one date (lower).

In a second phase, Support Vector Machine classifications are first applied to temporal entropy to extract 5 different classes characterising change detection based on previous change detection analysis, classes A, B, C, D and one stable class (figure 6). To carry out this SVM classification we select polygons over the 5 classes over the colour composition of figure 5b. We extract 500 training points by stratified random sampling. Then cross validation is performed in order to optimize the RBF kernel parameters. This classification is then used to build a mask between only stable and flooded area. Due to the very important contrast between the 5 classes under the temporal entropy we are very confident to the accuracy of the final mask, which explains why we do not conduct any accuracy assessment at this stage.

Secondly, to determine thematic classes most represented over the study area (shown in Table 3) that are affected by flood, we apply an SVM classification for each PALSAR database.

Reference maps for each date were drafted, which suggested the same land cover classes (8 classes shown in table 3). Differences between dates were recorded because of the fact that the local water level changed considerably between the four dates. The same thematic classes were used (table 3), but the water level altered the polarimetric response, which accounts for the differences between the floodable classes on certain dates (for instance, June 15, 2009 includes several classes in the floodable areas).

Examination of the different colour composites permitted the definition of classes of interest for flooded and floodable class identification (table 3). We identified a forest class within the stable entropy classification classes, a mixed phragmites class that is also included in the stable classes, a less dense class represented by short vegetation included in the floodable class and classes that changed considerably between 15 June 2009 and 18 June 2010. Other land cover floodable classes were identified: dunes and interdune depressions, hydrophilic vegetation (*Typha*, *Carex*), psammophilic vegetation (*Euphorbia*), halophilic vegetation (*Salicornia*). These classes were correlated with the flood classes and the floodable areas (table 3). Following is a description of the land cover of the region of Caraorman.

In terms of flooding regime, connectivity and groundwater residence times at a particular level, hydrology plays an important role in vegetation and soil distribution in the Danube Delta. The inter-dune depressions of Caraorman are supplied by fresh groundwater tables, without however being flooded by the river. The vegetation of the dunes is steppe vegetation and includes *Carex colchia*, sea grape (*Ephedra distachya),* forest rye *(Secale silvestra*), *Elymus giganteus* and *Festuca beckeri*. The fresh groundwater depressions are covered by rosemary leaf willow shrubs (*Salix rosmarinifolia*), by trees such as oak trees (*Quercus pedunculiflora*) and Pallis' ash (*Fraxinus pallisae*). Isolated *Quercus robur* and *Fraxinus angustifolia* also occur here. The groundwater level is several decimeters above sea level during the floods and 1.2 m to 1.4 m below sea level during the dry season. On the outskirts of the Caraorman region there are lower areas with salty and shallow groundwater tables. This assumption is supported by the presence of salt-tolerant vegetation: *Puccinellia convoluta*, Siberian statice (*Limonium gmelinii), sea rush (Juncus maritimus),* gouan *(Aeluropus littoralis).* These species are mixed with less salt-tolerant pasturelands and with shrubs like Salt Cedar (*Tamarix ramosissima),* Russian olive (*Elaeagnus angustifolia)* and common sea-buckthorn (*Hippophae rhamnoides).* The outskirts of the Caraorman region are more frequently and more heavily flooded. Vegetation progressively ranges from salt-tolerant vegetation to salty pasturelands including *Cyperaceae* and *Typha angustifolia* family plants, which are finally replaced by reed and sedge on the peat.

In the freshwater section of the delta (western area on our image), flood banks separate the distributaries of the river from the swamp. During the flood season (between mid-April and mid-June), the vegetation prevents suspended sediment distribution. A large amount of sediments, including fine sand, is deposited on the flood banks. The forest specific to floodable areas, made up of ash trees and poplars, is the natural flood bank vegetation where the floods season lasts less than 3 months. Higher flood banks are occupied by forests or meadows; they both prefer a well-drained alluvial soil, which has very little limestone (limestone fluvisol). At lower altitudes, the forest and meadows are on a mineral soil. Wetland depressions (swamps) are dominated by reed and sedge on gleysols which are often flooded. Floodable area forests also occur around lakes alternately with reed and sedge. The significant organic productivity of the standing water of the swamps, the small amount of sediments and the long-term floods lead to peat formation in the hydromorphic alluvial histic soils (peat formed on the *Sphagnum* moss). On this soil, reed (*Phragmites australis*) is 4 to 6 m high and mixed with *Typha angustifolia.*

Table 3.
Correspondence between classification results and flood classes.

Classes	Description
Submerged: lakes, branches, canals	Permanent waters
Flooded	Flooded between May 20, 2010 and June 8, 2010
Floodable	Short vegetation (grassland), hydrophilic vegetation, psammophilic vegetation, mixed vegetation, mixed phragmites, forest, dominant phragmites, cut phragmites
Drained until August 3, 2010	Flooded on June 18, 2010 and drained until August 3, 2010

The SVM model is only defined on the trained classes of the 2009 dataset. The SVM model defined for this date can be applied to the other PALSAR data because PALSAR calibrations are known to be good and also because we used exactly the same processing chain for each date. As for previous SVM classifications we apply a cross validation process in order to improve RBF kernel parameters. The creation of training and control point sets is the result of a stratified random sampling based on the whole set of areas of interest initially determined. A total of 500 training points and 800 control points are set for each class.

The results shown in table 4 reveal a good mean accuracy of 87%. In details we obtain very good performance of 95 % for the water class, hence the interest for flood monitoring uses. We noted some confusion between short vegetation and mixed vegetation classes, where the performance does not exceed 82 %. All the other classes show good performance levels (above 82 %).

Table 4.
Classification performance.

Class	Accuracy (percent)
Forest	89
Lake	95
Mixed phragmites	94
Short vegetation	82
Typha sp.	87
Mixed vegetation	82
Cut phragmites	85
Dominant phragmites	84

Mean accuracy	87

The stable classes (forest, delta lakes, cut phragmites, dominating phragmites) are well detected, whereas the flooding classes change the most (short vegetation (grasslands), mixed vegetation, hydrophilic vegetation, psammophilic vegetation, halophilic vegetation). Land cover maps are shown in figure 7 where we overlay Masked Classification (floodable areas were extracted from 2009/June 2010 dataset) into an image representing the mean of the intensity values on the dates taken into consideration. As shown in this figure non-floodable area shown in gray and blue are really well discriminated to floodable area.

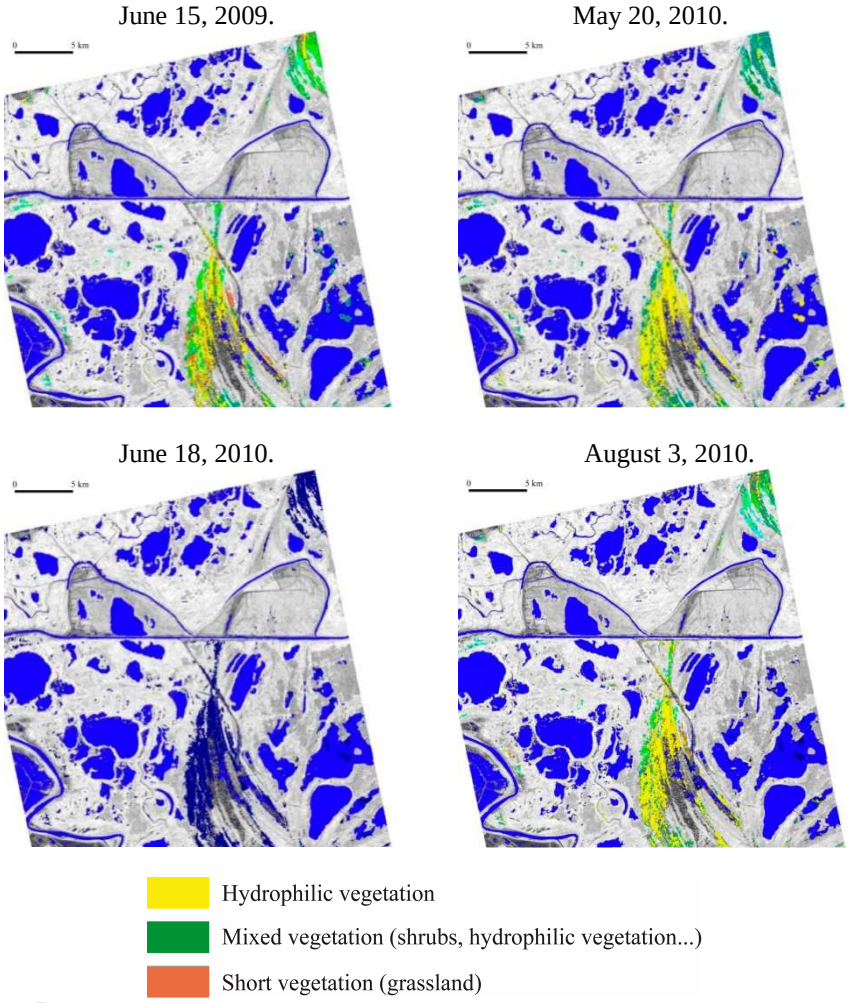

Figure 7.
Diachronic evolution of the four dates: before, during and after flooding. The three images acquired prior to and after the floods represent the floodable classes according to the flooded thematic mask extracted from the image of June 18, 2010. The stable classes are in grey.

Furthermore, work in progress leads us to believe that the performance attained by double polarisation radar images in L-band (PALSAR) in this study is superior to the performance obtained by optical imaging. The L-band wave penetration capacity is particularly suitable for water-level variation detection, even underneath vegetation cover, such as reeds in the Danube delta. This penetration also enhances the detection of the flood areas beneath the canopies. On the other hand, optical imaging only allows the detection of the response of the analysed area, and hence, it is not directly sensitive to water-level variation.

6. Conclusions and Perspectives

The objective of this paper is to contribute to and improve flood-prone and flooded area characterization in wetlands by means of satellite data acquired by L band polarimetric radars (ALOS-PALSAR). Polarimetric decomposition algorithms allow accurate polarimetric information extraction compared to a multi-polarized approach based on the HH and HV polarisation channels. Results clearly show that radar polarimetry always improves classification as compared to the HH and HV polarization channels. This improvement is sometimes marginal for certain “simple classes” such as bare soils, water or classes bearing a high proportion of volume backscattering. Nevertheless, radar polarimetry proves its full potential for the classes with more than one backscattering mechanism, generally a mechanism associated with plant structure and another one associated with substrate structure.

This paper provides a methodology for detecting changes using temporal entropy applied to the evaluation of flooded and floodable areas during the Danube delta floods of 2010. Changes were examined at the shortest possible time intervals before and after a flood. These application examples suggest that change detection is possible and could play a fundamental role in the process of understanding, in a broad sense of the term, the temporal evolution of a flooded or floodable landscape via sequential analysis.

Temporal entropy calculated from polarimetric indices is an easy way of detecting changes in the areas under investigation, and their comparison makes it possible to conduct a relevant qualitative analysis. Consequently, the analysis of the studied areas enabled us to detect the information most closely related to the changes of interest and least dependent on spatial variations (water level and vegetation cover). The use of SVM to classify change detection and to characterise the land cover using, respectively, temporal entropy and polarimetric indices for each acquisition, revealed the major contribution of the land cover based on floodable area

classification. The use of polarimetric data helped in the detection of structural differences between the various hydrophilic plant covers and, thus, contributed to the mapping of these types of areas in relation to the water level. It also provided additional information on the spatial extent of the flooded areas. Our paper shows that polarimetric indices allow better characterization, separabilities and classifications of the plant classes specific to floodable wetlands than the HH and HV polarization channels.

Regarding the future perspectives of our work, towards investigating the influence of wavelength on flood detection, we intend to conduct a multitemporal full polarisation RADARSAT-2 data analysis. In addition, it may be interesting to draw a comparison between dual PALSAR wavelengths (L-band) and RADARSAT-2 wavelengths (C-band) and to document the complementarity of the two instruments/sensors used to detect the land cover of floodable areas. Another line of research would include water level determination. Due to the interferometry principle, SAR data also allow water level determination, including under trees, with high accuracy. This information may prove interesting for estimating the amounts of stored water and for identifying major water level variations in wetlands.

References

Bonn, F., and R. Dixon, 2005. Monitoring flood extent and forecasting excess runoff risk with RADARSAT-1 data, Nat. Hazards, 35, pp 377–393.

Brivio P. A., Colombo R., Maggi M., and Tomasoni R., 2002. Integration of remote sensing data and GIS for accurate mapping of flooded areas, Int. J. Remote Sens., vol. 23, no. 3, pp 429–441.

Burges C-J, 1998. A tutorial on support vector machines for pattern recognition. Data mining and knowledge discovery, U. Fayyad, Ed. Kluwer Academic, pp 1-43.

Cameron W.L., Youssef N., and Leung L.K., 1996. Simulated polarimetric signatures of primitive geometrical shapes. IEEE Transactions on Geoscience and Remote Sensing, vol. 34, no. 3, pp 793-803.

Cloude S. R. and Pottier E., 1997. A review of target decomposition theorems in radar polarimetry. IEEE Transactions on Geoscience and Remote Sensing, vol. 34, no. 1, pp 68-78.

Cloude S., 2007. The Dual Polarization Entropy/Alpha Decomposition: A PALSAR Case Study. Proceedings: January 2007, Frascati, Italy.

Freeman A. and Durden S. L., 1998. A three-component scattering model for polarimetric SAR data. IEEE Transactions on Geoscience and Remote Sensing, vol. 36, no. 3, pp 963-973.

Fuchs M., Hoffmann R., Schwonke F., 2008. Change Detection with GRASS GIS - Comparison of images taken by different sensor. http://geoinformatics.fsv.cvut.cz/gwiki/Change_Detection_with_GRASS_GIS_ _Comparison_of_images_taken_by_different_sensors.

Fukuda S. and Hirosawa H., 2001. Support vector machine classification of land cover: application to polarimetric SAR data. Geoscience and Remote Sensing Symposium, 1, pp 187-189.

Gan T Y, Zunic F, Kuo C-C and Strobl T 2012 Flood mapping of Danube River at Romania using single and multi-date ERS2-SAR images, Int. J. Appl. Earth Obs. Geoinform.18, pp 69–81.

Gastescu P., Stiuca R., Delta Dunarii. Rezervatie a biosferei. Edition CD PRESS, 2008, 400p.

GIEC, 2014. Fifth Assessment Report - Mitigation of Climate Change – IPCC.

Hanganu J., Dubyna D., Zhmud E., Grigoras¸ I., Menke U., Drost H., Sefan N., Sarbu, I., 2002. Vegetation of the Biosphere Reserve “Danube Delta - with Transboundary Vegetation Map on a 1:150,000 scale. Danube Delta National Institute, Romania; M.G. Kholodny - Institute of Botany & Danube Delta Biosphere Reserve, Ukraine and RIZA, The Netherlands. RIZA report 2002.049 2002, 89 p.

Horritt M. S., Mason D. C. and Luckman A. J., 2001. Flood boundary delineation from synthetic aperture radar imagery using a statistical active contour model, Int. J. Remote Sens., 22:13, 2489–507.

Huang S., Cai X., Chen C. and Liu D., 2011. Change detection method based on fractal model and wavelet transform for multitemporal SAR images. Int. J. Appl. Earth Obs. Geoinform., 13, pp 863–72.

Inglada J. and Mercier G., 2007. A New Statistical Similarity Measure for Change Detection in Multitemporal SAR Images and its Extension to Multiscale Change Analysis. IEEE Transactions on Geoscience and Remote Sensing, vol. 45 (5) pp 1432-1446.

Jensen J.R., 2004. Introductory digital image processing - a remote sensing perspective. 3^{e} édition, Prentice Hall, Upper Saddle River, NJ, 316 p.

Krogager E., 1999. New decomposition of the radar target scattering matrix. IEEE Transactions on Geoscience and Remote Sensing, vol. 26, no. 18, pp 1525-1527.

Kussul N., Shelestov A. and Skakun S., 2008. Grid system for flood extent extraction from satellite images, Earth Sci. Inform., 1, pp 105–17.

Laugier O., Fellah K., Tholey N., Meyer C., and De Fraipont P., 1997. High temporal detection and monitoring of flood zone dynamic using ERS data around catastrophic natural events: The 1993 and 1994 Camargue flood events, paper presented at 3rd ERS Symposium on Space at the Service of Our Environment, Eur. Space Agency, Florence, Italy.

Lee J. S., Grunes M. R, de Grandi G., 1999. Polarimetric SAR speckle filtering and its implication for classification. IEEE Transactions on Geoscience and Remote Sensing, vol. 37, no. 5, pp 2362-2373.

Lee J.S. and Pottier E., 2009. Polarimetric radar imaging: from basics to applications. Brian J. Thompson, New York.

Lu D., Mausel P., Brondizio E. and Moran E., 2004. Change detection technique. International Journal of Remote Sensing, vol. 25, n°12, pp 2365-2407.

Lunetta R.S. and Elvidge C.D., 1998. Remote sensing change detection, environmental monitoring methods and applications. Ann Arbor Press, Ann Arbor (Michigan) 318 p.

Mas J.F., 2000. Une revue des méthodes et des techniques de télédétection du changement. Journal canadien de télédétection, vol. 26, n°4, pp 349-362.

Martinis S., Twele A. and Voigt S., 2009. Towards operational near real-time flood detection using a split-based automatic thresholding procedure on high resolution TerraSAR-X data. Natural Hazards Earth Syst., Sci. 9, pp 303–314.

Matgen, P., Schumann, G., Henry, J.B., Hoffmann, L. and Pfister, L., 2007. Integration of SAR-Derived Inundation Areas, High Precision Topographic Data and a River Flow Model Toward Real-Time Flood Management, Journal of Applied Earth Observation and Geoinformation, 9, pp 247–263.

Matgen P., Hostache R., Schumann G., Pfister L., Hoffman L. and Savenije H., 2011. Towards an automated SAR-based flood monitoring system: lessons learned from two case studies. Phys. Chem. Earth, 36, pp 241–52.

Niculescu S., Lardeux C., Frison J.L., Rudant J.P., 2009. Approche Sociale et Radar de la Gestion du Risque d'Inondation dans le delta du Danube, Houille Blanche, Revue Internationale de l'eau, SHF, Paris, n° 2.

Niculescu S., Lardeux C., Güttler Nor F., Rudant J.P., 2010. Multisensor systems and flood risk management. Application to the Danube Delta using radar and hyperspectral imagery, Remote Sensing, vol. 9, n°3-4.

Oberstadler, R., H. Hönsch, and D. Huth, 1997. Assessment of the mapping capabilities of ERS-1 SAR data for flood mapping: A case study in Germany, Hydrol. Processes, 10, pp 1415–1425.

Papathanassiou K. P. and Cloude S. R., 2001. Single-baseline polarimetric SAR interferometry. IEEE Transactions on Geoscience and Remote Sensing, vol. 39, no. 11, pp 2352-2363.

Schumann GJ-P, Di Baldassarre G, Bates P. D., 2009. The utility of space-borne radar to render flood inundation maps based on multi-algorithm ensembles. IEEE Trans Geosci Remote Sens, 47(8):2801–7.

Singh A., 1989. Digital change detection techniques using remotely-sensed data: Review article. International Journal Remote Sensing, vol. 10, no6, pp 989-1003.

Quin G., Pinel-Puysségur B, and Nicolas J.-M., 2012. Comparison of harmonic, geometric and arithmetic means for change detection in SAR time series. EUSAR. 9th European Conference on Synthetic Aperture Radar.

Touzi R., 1997. Target scattering decomposition in terms of roll invariant target parameters. IEEE Transactions on Geoscience and Remote Sensing, vol. 45, no. 1, pp 73-84.

Touzi R. and Charbonneau F., 2002. Characterization of target symmetric scattering using polarimetric, SAR. IEEE Transactions on Geoscience and Remote Sensing, vol. 40, no. 11, pp 693-711.

Van Zyl J.J., 1989. Unsupervised classification of scattering behavior using polarimetric data. IEEE Transactions on Geoscience and Remote Sensing, vol. 27, no. 1, pp 36-45.

Yajima Y., Yamaguchi Y., Sato R., Yamada H. and Boerner W.-M., 2008. PALSAR Image Analysis of Wetlands Using a Modified Four-Component Scattering Power Decomposition. IEEE Transactions on Geoscience and Remote Sensing, vol. 46, no. 6, pp 1667-1673.